Ultraefficient Coupling of a Quantum Emitter to the Tunable Guided Plasmons of a Carbon Nanotube

Luis Martín-Moreno,[1,*] F. Javier García de Abajo,[2,3,†] and Francisco J. García-Vidal[4,5]

[1]*Instituto de Ciencia de Materiales de Aragón and Departamento de Física de la Materia Condensada, CSIC-Universidad de Zaragoza, E-50009 Zaragoza, Spain*
[2]*ICFO—Institut de Ciencies Fotoniques, The Barcelona Institute of Science and Technology, 08860 Castelldefels (Barcelona), Spain*
[3]*ICREA—Institució Catalana de Recerca i Estudis Avançats, Passeig Lluís Companys 23, 08010 Barcelona, Spain*
[4]*Departamento de Física Teórica de la Materia Condensada and Condensed Matter Physics Center (IFIMAC), Universidad Autónoma de Madrid, E-28049 Madrid, Spain*
[5]*Donostia International Physics Center (DIPC), E-20018 Donostia/San Sebastian, Spain*

We show that a single quantum emitter can efficiently couple to the tunable plasmons of a highly doped single-wall carbon nanotube (SWCNT). Plasmons in these quasi-one-dimensional carbon structures exhibit deep subwavelength confinement that pushes the coupling efficiency close to 100% over a very broad spectral range. This phenomenon takes place for distances and tube diameters comprising the nanometer and micrometer scales. In particular, we find a β factor ≈ 1 for QEs placed 1–100 nm away from SWCNTs that are just a few nanometers in diameter, while the corresponding Purcell factor exceeds 10^6.

PACS numbers: 42.50.Ex, 33.50.-j, 73.20.Mf, 78.67.Ch

Achieving an efficient coupling between a single quantum emitter (QE) and the surface plasmons (SPs) supported by metallic nanostructures has become a popular subject of research due to its potential application to quantum-optics [1–3] and sensing [4,5]. This efficient coupling lies at the heart of several surface-based ultrasensitive optical analysis techniques, which rely on the plasmon-driven enhancement of Raman scattering [4] and infrared absorption [5]. Remarkably, the *localized* SPs of a metal nanoparticle can enormously modify the spontaneous decay of a neighboring excited molecule [6–8], while *propagating* SPs can produce similar effects over a broadband spectral range. Reducing the dimensionality of the plasmonic structure from 2D (metal surfaces) to 1D (thin wires) enables better control over the coupling, which can be engineered to affect just a single SP [2]. Additionally, the SPs of 1D geometries are well suited to act as mediators in the interaction between several QEs placed in close proximity to a plasmonic waveguide [9–12], thus suggesting the combination of these tools to design large-scale quantum-optics integrated devices, which could benefit from the plasmon robustness against environmental fluctuations to operate under ambient conditions.

The recent emergence of graphene as a plasmonic material [13–15] has introduced an additional knob to improve the performance of QE-SP coupling. The large electrical tunability and high degree of confinement recently measured in graphene plasmons [16–20] has stimulated suggestions for their use in tunable plasmonic circuitry and metamaterials [21], as well as for the achievement of quantum strong coupling and efficient interaction with QEs [22,23] with superior performance compared with conventional plasmonic metals. Although these plasmons

have been so far observed only at midinfrared and lower frequencies, their extension towards the more technologically appealing spectral ranges of the visible and near-infrared has been argued to be attainable [24], particularly by reducing the size of the structures to scales of a few nanometers, which are commensurable with existing graphene-related structures such as aromatic molecules [25] and carbon nanotubes. In particular, nanotubes of tens of nanometers in diameter have been recently suggested as suitable elements for plasmon circuitry [26]. It should be noted that SWCNTs, like other carbon allotropes, exhibit UV plasmons that have been well characterized in the past [27]. However, those plasmons are much lossier, and therefore less prone to efficiently couple to QEs, than the tunable lower-energy plasmons on which we concentrate here, which only exist in doped structures and are predicted to display similar electrical tunability as graphene.

In this Letter, we show that quantum emitters can strongly couple to the electrically tunable plasmons of doped SWCNTs, reaching light-matter interaction levels that go even beyond those of planar graphene. From the THz to the midinfrared frequency range, the Purcell factor (i.e., the decay rate near the material, normalized to the decay rate in free space) is increased by nearly 3 orders of magnitude when reducing the dimensionality of the carbon nanostructure from 2D (graphene) to quasi-1D (nanotubes). More importantly, the coupling efficiency of the QE to the SPs supported by SWCNTs (i.e., the fraction of decay into SPs, also known as β factor) reaches values nearing 100% over a very broad range of QE-SWCNT distances and QE/SP frequencies. At higher frequencies, Purcell and beta factors are similar for emitters close to either graphene or a SWCNT; even in this case the use of SWCNT opens
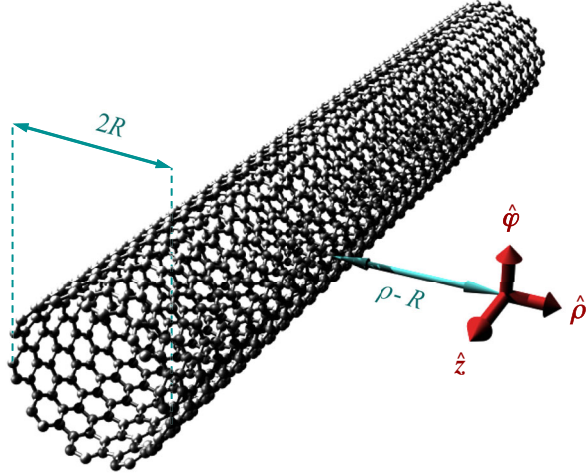
FIG. 1 (color online).   Sketch of the system under study. We consider a QE placed at a distance $\rho - R$ from the surface of a SWCNT of radius R. Three orthogonal orientations of the emitter dipole **p** are considered, as shown by the red arrows.

additional possibilities because it presents a favorable dependence of the interaction on the distance compared with planar materials.

Figure 1 depicts the system under study: a single QE placed at a distance ρ from the axis of a SWCNT of radius R. The emission properties of the QE are determined by its transition frequency ω and dipole moment **p**. We assume that R is sufficiently large as to neglect curvature effects (i.e., the discreteness of the electronic bands, as well as features near the Dirac point associated with the tube chirality and finite radius). A recent study [24] indicates that this approximation works well and tube chirality effects can be neglected in the description of transversal plasmons for $R > 1$ nm under the doping conditions here considered (see below) down to the near-infrared spectral region, although narrower nanotubes require a more fundamental level of description [28,29]. SWCNTs have been synthesized in this size range [30] and their excitonic absorption bands well characterized [31–33]. We thus model the SWCNT as a hollow tube with the same surface conductivity $\sigma(\omega)$ as graphene doped with the considered number of charge carriers per carbon atom. This is convenient, as it allows us to readily compare 2D graphene and 1D SWCNTs. From a more quantitative point of view, our choice is justified in the Supplemental Material [34], where we show that the computed extinction cross section of SWCNT is very similar when using the local limit of the random-phase approximation (RPA) for $\sigma(\omega)$ in graphene [39,40] and the numerically computed RPA for the SWCNT [38]. In all calculations presented in this paper, we use realistic values for the chemical potential $\mu_c = 1$ eV, corresponding to 1 charge carrier per every 52 carbon atoms, and the plasmon relaxation time $\tau = 1$ ps, and consider that the temperature is T = 300 K. A set of calculations for $E_F = 0.5$ eV can be found in the Supplemental Material [34], showing the robustness of the effects predicted in this work.

Importantly, SPs within this model are insensitive to the sign of the doping, and the relative comparison between 2D and 1D geometry is independent of the choice of τ. However, the high Purcell factor here predicted (see below) is roughly proportional to the assumed τ.

In this work we are most interested in situations in which both R and ρ are small compared with the light wavelength λ. Therefore, the electrostatic limit here outlined, which leads to relatively affordable analytical expressions, provides a very accurate level of description, as shown below. A comparison between results obtained with the electrostatic approach and a full electromagnetic formalism (whose derivation is given in [34]) is presented in Fig. 2, whereas both approaches give nearly identical results on the scale of Figs. 3 and 4.

We start our analysis by considering the screened interaction $W(\mathbf{r}, \mathbf{r}', \omega)$, defined as the electric scalar potential created at the position $\mathbf{r}$ by an oscillating point charge $\exp(-i\omega t)$ placed at $\mathbf{r}'$. Reciprocity implies that $W(\mathbf{r}, \mathbf{r}', \omega)$ is symmetric with respect to the exchange of $\mathbf{r}$ and $\mathbf{r}'$. Also, it is convenient to decompose $W(\mathbf{r}, \mathbf{r}', \omega) = 1/|\mathbf{r} - \mathbf{r}'| + W^{\text{ind}}(\mathbf{r}, \mathbf{r}', \omega)$ as the sum of bare and induced interactions. This quantity allows us to obtain the plasmon characteristics, as well as the decay rate of a neighboring QE. Direct solution of Poisson's equation for both $\mathbf{r}$ and $\mathbf{r}'$ placed outside the tube yields [34]

$$W^{\text{ind}}(\mathbf{r}, \mathbf{r}', \omega) = \frac{2}{\pi} \sum_{m=0}^{\infty} (2 - \delta_{m0}) \cos[m(\varphi - \varphi')]$$
$$\times \int_0^{\infty} dk\, r_m(k) \cos[k(z - z')] K_m(k\rho) K_m(k\rho'),$$
(1)

where we use cylindrical coordinates $\mathbf{r} = (\rho, z, \varphi)$,

$$r_m(k) = \frac{-I_m^2(kR)\Delta_m}{1 + I_m(kR)K_m(kR)\Delta_m}$$
(2)

is the reflection coefficient for cylindrical waves, $\Delta_m = (4\pi i\sigma/\omega R)(m^2 + k^2 R^2)$, and I_m and K_m are modified Bessel functions. The integral in Eq. (1) is performed over the wave vector k parallel to the axis of the nanotube, while the sum runs over components of fixed azimuthal angular momentum number m.

Plasmon resonances are signaled by their strong response for a given external perturbation, or equivalently, by the poles of $r_m(k)$. Here we should note that sign cancellations due to the $\exp(im\varphi)$ modulation of the induced charge along the azimuthal direction of the tube surface render the contribution of $m \neq 0$ modes small if ρ is larger than the radius R. We thus concentrate on the dominant $m = 0$ plasmon band, whose complex wave vector k_p is found as a function of frequency ω from the solution to the transcendental equation
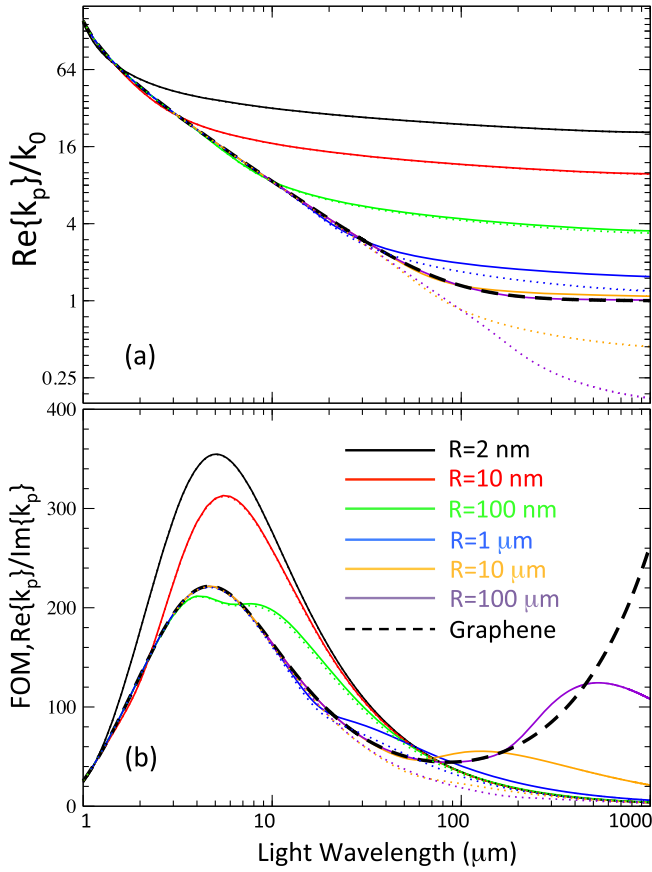
FIG. 2 (color online). Propagation characteristics of plasmons supported by SWCNTs and the limit towards graphene. (a) Real part of the plasmon wave vector k_p as a function of the wavelength λ of free-space light oscillating at the same frequency for different values of the tube radius R. The plasmon wave vector is normalized to the light wave vector $k_0 = 2\pi/\lambda$. The limit of 2D graphene (dashed curve) is smoothly approached at large R's. (b) The corresponding figure of merit (FOM) $\text{Re}\{k_p\}/\text{Im}\{k_p\}$ of the guided plasmons studied in (a). Full electromagnetic theory (solid curves) is compared with the electrostatic limit (dotted curves) in both panels.

$$\frac{\omega}{\sigma(\omega)} = -4\pi i R k_p^2 I_0(k_p R) K_0(k_p R).$$

For $\hbar\omega \ll 2E_F$, when the conductivity is dominated by the intraband (Drude) term, and in the limit $\tau \to \infty$, this transcendental equation becomes $\omega^2 = (4e^2 E_F/\hbar^2) I_0(k_p R) K_0(k_p R) k_p^2 R$, which agrees with previous studies [41–43]. Here we consider the full RPA expression for the conductivity, including losses and interband transitions. In Fig. 2(a) we show $\text{Re}\{k_p\}$ as a function of light wavelength λ for SWCNTs of radius R in the 2 nm–100 μm range. This magnitude is normalized to the free-space light wave vector $k_0 = 2\pi/\lambda$, so that the plot directly illustrates the degree of spatial confinement of the plasmon, whose radial electric field is proportional to $K_1(k_p\rho)$. Whereas the case of small radius corresponds
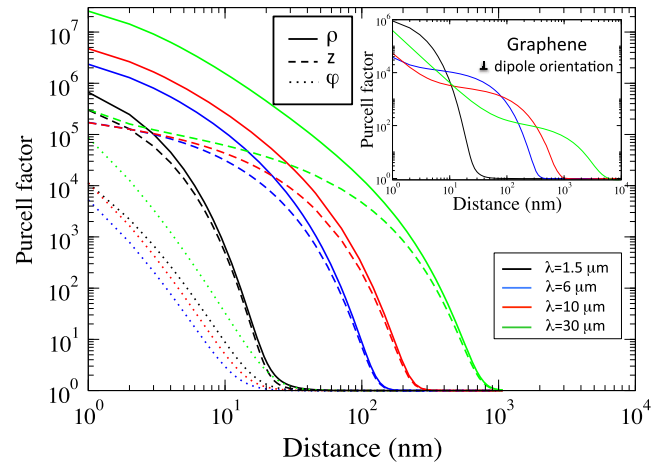

FIG. 3 (color online). Purcell factor. The main panel shows the Purcell factor [Eq. (4)] as a function of the distance $\rho - R$ from the QE to the surface of a SWCNT of radius $R = 2$ nm for several values of the free-space emission wavelength λ and all three possible QE dipole orientations (see Fig. 1): radial (continuous curves), longitudinal (dashed curves), and azimuthal (dotted curves). The inset shows the corresponding Purcell factor in graphene for the same wavelengths and a dipole orientation perpendicular to the carbon plane.

to realistic SWCNTs, we also consider very large R in order to deal with graphene-coated cylinders. In this way, this figure illustrates the evolution from small tubes to planar graphene with increasing R. For comparison, we further plot the dispersion relation of the SPs supported by a graphene sheet. As discussed above, the electrostatic limit yields very accurate results for nanotubes of small radius ($R < 100$ nm), and also for larger radius at short wavelengths. The results show that $\text{Re}\{k_p\}$ is virtually the same for graphene and carbon nanotubes for light wavelengths
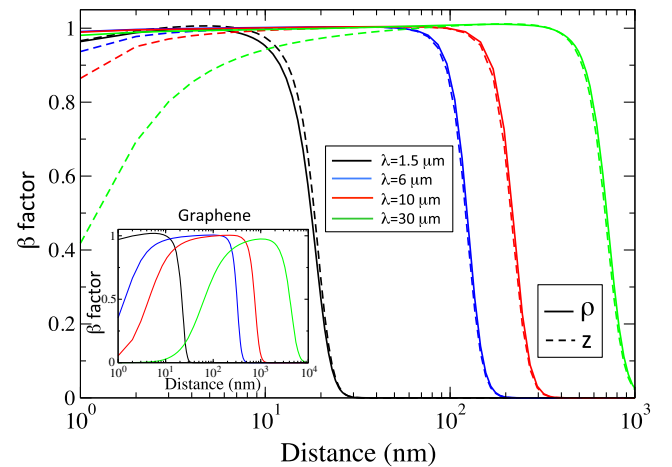

FIG. 4 (color online). β factor. Fraction of decay into SPs (β factor) from radially ($\|\rho$) and longitudinally ($\|z$) oriented QEs under the same conditions as in Fig. 3. The inset shows the β factor for a point dipole perpendicularly oriented to a 2D graphene sheet.

$\lambda \lesssim 1.5\ \mu m$, independently of its radius. However, for $\lambda > 1.5\ \mu m$, plasmons propagating along carbon nanotubes are more confined (larger $\mathrm{Re}\{k_p\}$) than those supported by graphene, and their confinement increases with decreasing R. This suggests that SWCNTs are better suited to produce enhanced coupling with QEs in this spectral range.

The ratio between the real and imaginary parts of k_p is also an important magnitude, typically used as a figure of merit (FOM=$\mathrm{Re}\{k_p\}/\mathrm{Im}\{k_p\}$) for evaluating the plasmon attenuation length of SPs. This FOM is plotted in Fig. 2(b) as a function of λ for SWCNTs of different radius R. Remarkably, these SPs possess a larger FOM than those of graphene for spectral and geometrical-parameter ranges in which they also exhibit tighter confinement, as noted above (see $1.5\ \mu m < \lambda < 100\ \mu m$ region). These characteristics are very beneficial for the design of efficient coupling schemes between several QEs mediated by SPs.

A convenient way of assessing the strength of the QE-SP coupling consists in analyzing the rate of spontaneous emission, Γ. In particular, the Purcell factor $P = \Gamma/\Gamma_0$, where Γ_0 is the decay rate in vacuum, is directly related to the ratio of the plasmon resonance quality factor to the mode volume. For a point dipole $\mathbf{p}$ located at $\mathbf{r}$, it can be calculated as [44]

$$P = 1 + \frac{3}{2p^2 k_0^3}\mathrm{Im}\{\mathbf{p} \cdot \mathbf{E}^{\mathrm{ind}}(\mathbf{r})\}, \qquad (3)$$

where $\mathbf{E}^{\mathrm{ind}}(\mathbf{r})$ is the field induced by the dipole at its own position, which can be in turn obtained from the screened interaction as $\mathbf{E}^{\mathrm{ind}}(\mathbf{r}) = -\vec{\nabla}_{\mathbf{r}}[(\mathbf{p} \cdot \vec{\nabla}_{\mathbf{r}'})W^{\mathrm{ind}}(\mathbf{r}, \mathbf{r}', \omega)]|_{\mathbf{r}'=\mathbf{r}}$. Using Eq. (1) and specifying for dipoles oriented along the three orthogonal directions shown in Fig. 1, we find

$$P_\rho = 1 - \frac{3}{\pi k_0^3}\sum_{m=0}^{\infty} b_m \int_0^{\infty} dk k^2 [K'_m(k\rho)]^2 \mathrm{Im}\{r_m(k)\}, \quad (4a)$$

$$P_z = 1 - \frac{3}{\pi k_0^3}\sum_{m=0}^{\infty} b_m \int_0^{\infty} dk k^2 K_m^2(k\rho)\mathrm{Im}\{r_m(k)\}, \qquad (4b)$$

$$P_\varphi = 1 - \frac{6}{\pi k_0^3}\sum_{m=1}^{\infty} c_m \int_0^{\infty} dk K_m^2(k\rho)\mathrm{Im}\{r_m(k)\}, \qquad (4c)$$

where $K'_m(z) = dK_m(z)/dz$, $b_m = (2 - \delta_{m0})$, and $c_m = m^2/\rho^2$. Incidentally, this formalism can be easily adapted to cope with QEs of non-negligible size compared with λ or ρ simply by considering a more delocalized transition current beyond the dipole approximation, leading to a modified form of Eq. (3), which might be useful to account for finite-size effects of infrared QEs [45].

In Fig. 3, we study the QE-SWCNT distance dependence of P_ρ, P_φ, and P_z for tubes of radius $R = 2$ nm and for several QE emission wavelengths λ in the 1.5–30 μm range. The highest Purcell factor is observed for radial

orientation, as expected from the $-1/\rho$ divergence of the induced field at small separations, whereas the azimuthal orientation renders poor coupling because it is only contributed by $m \neq 0$ SPs. The comparison between the Purcell factor associated with either SWCNTs or graphene (see inset to Fig. 3) for the corresponding optimal QE-dipole orientations (P_ρ for SWCNTs and perpendicular to the 2D carbon sheet for graphene) is revealing. As soon as λ is large enough so that the mode confinement is stronger in 1D SWCNTs than in 2D graphene, not only the Purcell factor is higher for the nanotube, but their spatial dependences are very different: whereas for graphene the Purcell factor increases rapidly towards short separations due to the dominant role of nonradiative channels, for SWCNTs this increase is much less pronounced.

As mentioned above, a high coupling efficiency between QEs and propagating SPs is a key ingredient to achieve many of the proposed functionalities within the field of waveguide QED. In Fig. 4 we show the β factor as a function of the QE-SWCNT distance for several values of the QE frequency. This magnitude can be evaluated by calculating the contribution of the SP pole to the integrals of Eq. (4). We evaluate the β factor near a SWCNT of radius $R = 2$ nm for the two optimal QE orientations, radial (ρ) and longitudinal (z). For comparison, we plot in the inset the evolution of the coupling efficiency for a QE near a graphene layer, with its dipole oriented perpendicularly to the 2D carbon plane. The coupling efficiency for SWCNTs reaches 100% over a very broad range of distances: for the optimal orientation (radial), β is close to 1 for distances ranging from 1 nm to 1 μm (spanning 3 orders of magnitude). Importantly, this high coupling efficiency extends over a very broad range of frequencies and is even larger in the very low frequency regime. Our results imply that the quenching phenomenon (i.e., when the QE emission is dominated by nonradiative decay channels) only appears at very short distances (<1 nm) for QEs coupled to SWCNTs. In opposition to other metallic systems, SWCNTs present the crucial advantage of not requiring a spacer to avoid quenching of QEs at small separations. We attribute this reduction of quenching to the very small quantity of material that binds the EM fields to the carbon nanotube. In contrast, in graphene a high coupling efficiency is only observed within a much narrower range of distances, and quenching shows up at distances below ~ 10 nm even for midinfrared frequencies (see inset of Fig. 4).

The strong interaction here predicted between QEs and the plasmons of SWCNTs opens new possibilities to implement waveguide QED schemes. It is worth noting that electrical contacts between gates and carbon nanotubes have been extensively studied for their potential as nanoelectronics elements, thus facilitating the design of practical electrical doping schemes. This combination of classical electrical tunability and efficient coupling with

QEs constitutes a powerful platform for the investigation of fundamental quantum physics and the design of devices capable of processing information encoded in the states of the QEs.

---

*lmm@unizar.es

†javier.garciadeabajo@icfo.es

[1] D. E. Chang, A. S. Sörensen, P. R. Hemmer, and M. D. Lukin, Phys. Rev. Lett. **97**, 053002 (2006).

[2] A. Akimov, A. Mukherjee, C. Yu, D. Chang, A. Zibrov, P. Hemmer, H. Park, and M. Lukin, Nature (London) **450**, 402 (2007).

[3] D. E. Chang, A. S. Sörensen, E. A. Demler, and M. D. Lukin, Nat. Phys. **3**, 807 (2007).

[4] S. Nie and S. R. Emory, Science **275**, 1102 (1997).

[5] J. Kundu, F. Le, P. Nordlander, and N. J. Halas, Chem. Phys. Lett. **452**, 115 (2008).

[6] P. Anger, P. Bharadwaj, and L. Novotny, Phys. Rev. Lett. **96**, 113002 (2006).

[7] S. Kühn, U. Håkanson, L. Rogobete, and V. Sandoghdar, Phys. Rev. Lett. **97**, 017402 (2006).

[8] A. Archambault, F. Marquier, J. J. Greffet, and C. Arnold, Phys. Rev. B **82**, 035411 (2010).

[9] D. Martin-Cano, L. Martín-Moreno, F. J. García-Vidal, and E. Moreno, Nano Lett. **10**, 3129 (2010).

[10] D. Dzsotjan, A. S. Sörensen, and M. Fleischhauer, Phys. Rev. B **82**, 075427 (2010).

[11] A. Gonzalez-Tudela, D. Martin-Cano, E. Moreno, L. Martín-Moreno, C. Tejedor, and F. J. García-Vidal, Phys. Rev. Lett. **106**, 020501 (2011).

[12] D. Dzsotjan, J. Kästel, and M. Fleischhauer, Phys. Rev. B **84**, 075419 (2011).

[13] G. W. Hanson, J. Appl. Phys. **103**, 064302 (2008).

[14] M. Jablan, H. Buljan, and M. Soljačić, Phys. Rev. B **80**, 245435 (2009).

[15] A. H. Castro Neto, F. Guinea, N. M. R. Peres, K. S. Novoselov, and A. K. Geim, Rev. Mod. Phys. **81**, 109 (2009).

[16] Z. Fei, G. O. Andreev, W. Bao, L. M. Zhang, A. S. McLeod, C. Wang, M. K. Stewart, Z. Zhao, G. Dominguez, M. Thiemens et al., Nano Lett. **11**, 4701 (2011).

[17] J. Chen, M. Badioli, P. Alonso-González, S. Thongrattanasiri, F. Huth, J. Osmond, M. Spasenović, A. Centeno, A. Pesquera, P. Godignon et al., Nature (London) **487**, 77 (2012).

[18] Z. Fei, A. S. Rodin, G. O. Andreev, W. Bao, A. S. McLeod, M. Wagner, L. M. Zhang, Z. Zhao, M. Thiemens, G. Dominguez et al., Nature (London) **487**, 82 (2012).

[19] Z. Fang, S. Thongrattanasiri, A. Schlather, Z. Liu, L. Ma, Y. Wang, P. M. Ajayan, P. Nordlander, N. J. Halas, and F. J. García de Abajo, ACS Nano **7**, 2388 (2013).

[20] V. W. Brar, M. S. Jang, M. Sherrott, J. J. Lopez, and H. A. Atwater, Nano Lett. **13**, 2541 (2013).

[21] A. Vakil and N. Engheta, Science **332**, 1291 (2011).

[22] F. H. L. Koppens, D. E. Chang, and F. J. García de Abajo, Nano Lett. **11**, 3370 (2011).

[23] A. Y. Nikitin, F. Guinea, F. J. García-Vidal, and L. Martín-Moreno, Phys. Rev. B **84**, 195446 (2011).

[24] F. J. García de Abajo, ACS Photon. **1**, 135 (2014).

[25] A. Manjavacas, F. Marchesin, S. Thongrattanasiri, P. Koval, P. Nordlander, D. Sánchez-Portal, and F. J. García de Abajo, ACS Nano **7**, 3635 (2013).

[26] I. Soto Lamata, P. Alonso-Gonzalez, R. Hillenbrand, and A. Y. Nikitin, ACS Photon. **2**, 280 (2015).

[27] O. Stéphan, D. Taverna, M. Kociak, K. Suenaga, L. Henrard, and C. Colliex, Phys. Rev. B **66**, 155422 (2002).

[28] G. Y. Guo, K. C. Chu, D. S. Wang, and C. G. Duan, Phys. Rev. B **69**, 205416 (2004).

[29] R. S. Swathi and K. L. Sebastian, J. Chem. Phys. **132**, 104502 (2010).

[30] J. Ma, J. N. Wang, and X. X. Wang, J. Mater. Chem. **19**, 3033 (2009).

[31] M. Y. Sfeir, T. Beetz, F. Wang, L. Huang, X. M. H. Huang, M. Huang, J. Hone, S. O'Brien, J. A. Misewich, T. F. Heinz et al., Science **312**, 554 (2006).

[32] J.-C. Blancon, M. Paillet, H. N. Tran, X. T. Than, S. A. Guebrou, A. Ayari, A. San Miguel, N.-M. Phan, A.-A. Zahab, J.-L. Sauvajo et al., Nat. Commun. **4**, 2542 (2013).

[33] K. Liu, X. Hong, S. Choi, C. Jin, R. B. Capaz, J. Kim, S. Aloni, W. Wang, X. Bai, S. G. Louie et al., Proc. Natl. Acad. Sci. U.S.A. **111**, 7564 (2014).

[34] See Supplemental Material at http://link.aps.org/supplemental/10.1103/PhysRevLett.115.173601 for (i) a validation of the conductivity model used, (ii) the derivation of both quasistatic and full electromagnetic responses, and (iii) a similar study to that presented in the main text, but at $\mu_c = 0.5$ eV, which includes Refs. [35–38].

[35] J. D. Jackson, Classical Electrodynamics (Wiley, New York, 1999).

[36] M. Abramowitz and I. A. Stegun, Handbook of Mathematical Functions (Dover, New York, 1972).

[37] C.-T. Tai, Dyadic Green Functions in Electromagnetic Theory (IEEE Press Series on Electromagnetic Waves, New York, 1994).

[38] S. Thongrattanasiri, A. Manjavacas, and F. J. García de Abajo, ACS Nano **6**, 1766 (2012).

[39] B. Wunsch, T. Stauber, and F. Guinea, New J. Phys. **8**, 318 (2006).

[40] L. A. Falkovsky, Phys. Usp. **51**, 887 (2008).

[41] P. Longe and S. M. Bose, Phys. Rev. B **48**, 18239 (1993).

[42] C. Yannouleas, E. N. Bogachek, and U. Landman, Phys. Rev. B **53**, 10225 (1996).

[43] X. Jiang, Phys. Rev. B **54**, 13487 (1996).

[44] L. Novotny and B. Hecht, Principles of Nano-Optics (Cambridge University Press, Cambridge, 2012).

[45] M. L. Andersen, S. Stobbe, A. S. Sorensen, and P. Lodahl, Nat. Phys. **7**, 215 (2011).